Advances in Computer, Signals and Systems (2023)
Clausius Scientific Press, Canada

DOI: 10.23977/acss.2023.070902
ISSN 2371-8838 Vol. 7 Num. 9

Model Predictive Control of Hydrogen Pressure of Multi-Stack Fuel Cell System

Zhou Su[a,*], Huang Zhiquan[b], Wang Ruoyi, Gao Jianhua

School of Automotive Studies, Tongji University, Shanghai, China
[a]autotongji_zhou@163.com, [b]ralphhzq@163.com
[*]Corresponding author

Keywords: Multi-stack fuel cell system; Proton exchange membrane fuel cell; Hydrogen system; Integrated recirculation; Model predictive control

Abstract: To control and stabilize the hydrogen pressure in a multi-stack fuel cell system, a dynamic simulation model of a multi-stack fuel cell hydrogen system structure containing supply and exhaust common rail is built based on Matlab/Simulink. In the control method, the idea of local linearization was adopted. Local linearization models of the system around different steady-state operating points were built and model predictive controller for each interval was designed. This multi-point linearized control model can improve the solution speed and reduce the impact caused by the mismatch problem. The results show that under step operating condition, the deviation of the reactor inlet pressure can be reduced by 22.5%, and the adjustment time can be reduced from 31 to 22 seconds. Under C-WTVC operating condition, power consumption of the blower in the hydrogen system is reduced by 13.6% compared with that of the conventional PID. It is concluded that the controller designed in this paper is better than the traditional PID controller and is more suitable for the hydrogen system of the multi-stack fuel cell.

1. Introduction

In recent years, proton exchange membrane fuel cells (PEMFC) powered by renewable hydrogen energy have become a focus of attention. These fuel cells have high efficiency, zero emissions, long endurance, high energy density, and fast refueling time[1]. In high-power applications, they have limitations because of stack size and output power. Therefore, fuel cell systems are developed from single-stack to multi-stack and their level of integration are continuously improved. Multi-stack fuel cell systems not only offer higher power output but also greater stability and slower aging, making them the direction for future development. Research related to multi-stack fuel cell systems (MFCS) is mainly based on the achievements of single-stack fuel cell systems (SFCS), but their structures and integrated designs for auxiliary systems differ significantly, especially in the arrangement of the fuel cell stacks[2]. Specific research on multi-stack fuel cell systems and their subsystems remains relatively scarce. Research on hydrogen sub-systems in single-stack fuel cells mainly concentrates on hydrogen pressure control and hydrogen circulation methods. Considering the commonality of hydrogen supply systems in both SFCS and MFCS, these studies provide valuable insights.

Yang et al.[3] conducted a comprehensive overview of control strategies for PEMFCs, categorizing

them into nine types and providing a comprehensive assessment and summary of control design, objectives, performance, applications, advantages/disadvantages, complexity, robustness, and accuracy. Regarding hydrogen inlet pressure control, Nie Wei et al.[4] analyzed the factors influencing hydrogen pressure control in fuel cell power systems and the flow characteristics of various components, using this as the basis to establish a mathematical pressure control model. They proposed a pressure control algorithm combining pressure PI control with load current feedforward control. He et al.[7] analyzed a hydrogen system parallel to the ejector and recirculation blower. They researched relationships between stack current and various state parameters and designed three control strategies: The results showed that state feedback control was the most optimal.

This paper will address the issue of limited research on hydrogen pressure control in multi-stack fuel cell systems. It is based on the dynamic simulation model of a multi-stack fuel cell hydrogen system and designs a model predictive controller. The control effectiveness of the designed controller is compared and analyzed against traditional controllers using step tests and C-WTVC tests.

2. The structure and modeling of the hydrogen system in a multi-stack fuel cell (MFCS)

2.1. The structure of the hydrogen system in a multi-stack fuel cell (MFCS)

The structure of the hydrogen system in the multi-stack fuel cell under study is shown in Figure 1. Hydrogen flows out from high-pressure hydrogen bottles into the supply common rail and is then directed to individual fuel cell stacks through proportional valves. Exhausted gas is recirculated from the exhaust common rail to the supply common rail through the combined action of an ejector and a recirculation blower. According to research [2], the three fuel cell stacks in this multi-stack fuel cell system have sizes of 20 kW, 70 kW, and 120 kW respectively, to meet the power requirements of the system at different power levels.

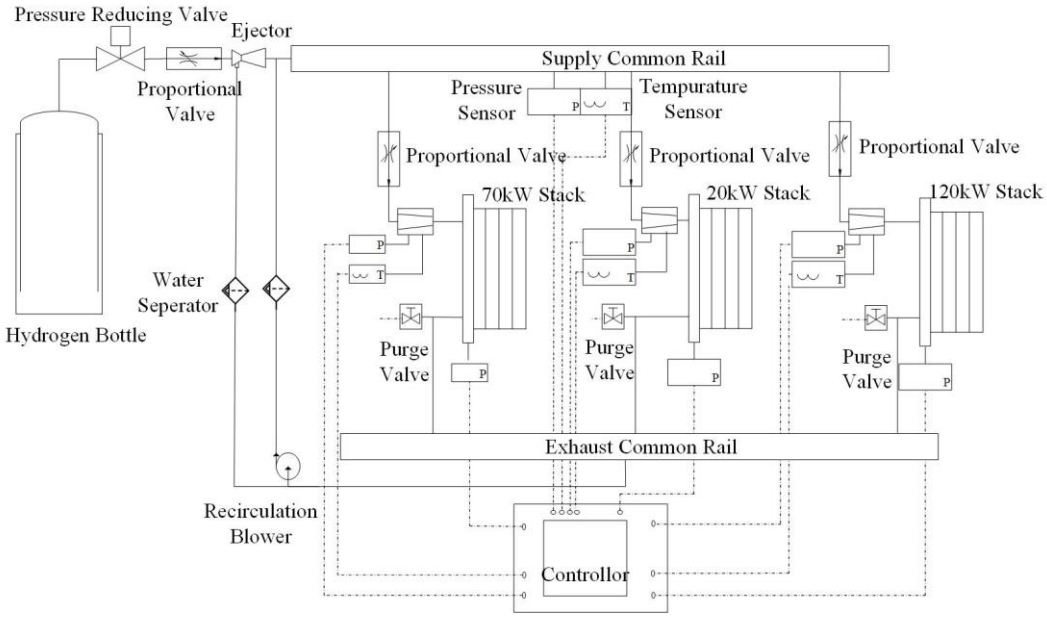

Figure 1: The structure of the hydrogen system in a multi-stack fuel cell (MFCS).

2.2. Fuel Cell and Hydrogen System Modeling

In the modeling process of the structure studied in this paper, the following assumptions [8] need to be made:

(1) It is assumed that the air sub-system is operating normally.

(2) It is assumed that all gases in the entire model are ideal gases, and the calculation formulas for ideal gases are applicable.

(3) It is assumed that the gas flowing out of the hydrogen bottles through the pressure reducing valve is pure hydrogen and that the pressure is stable.

(4) It is assumed that the gas flow paths and pipelines are adiabatic systems.

(5) It is assumed that the gas flow is steady laminar flow.

2.2.1. Anode Channel Model

In the anode channel, the mass changes of various components in the channel space can be represented by Equation (1):

$$\frac{dm_{Anode}}{dt} = \dot{m}_{Anode,in,H_2} - \dot{m}_{Anode,out,H_2} - \dot{m}_{reacted,H_2} - \dot{m}_{membrane,H_2} \tag{1}$$

In Equation (1), $\dot{m}_{Anode,in,H_2}$ and $\dot{m}_{Anode,out,H_2}$ are the mass flow rates entering and exiting the anode channel, kg/s; $\dot{m}_{reacted,H_2}$ represents the mass flow rate consumed by reactions, kg/s; $\dot{m}_{membrane,H_2}$ represents the mass flow rate due to membrane transport, kg/s. It is assumed that when the water content in the channel exceeds the maximum water vapor content, the excess exists in the form of liquid water[9].

Additionally, according to Faraday's law, the relationship between the fuel cell current and the mass flow rate of hydrogen reaction can be established as follows:

$$\dot{m}_{reacted,H_2} = n_{cell}\frac{M_{H_2} I_{FCS}}{2F} \tag{2}$$

In Equation (2), I_{FCS} is the fuel cell current, A; n_{cell} is the number of stacks in the fuel cell stack; M_{H_2} is the molar mass of hydrogen gas, kg/mol; F is the Faraday constant, 96,485.3 C/mol.

2.2.2. Supply and Exhaust Common Rail Model

According to the structure, the gases entering the supply common rail include pure hydrogen and a mixture returning from exhaust common rail, while the gases exiting are entering the three fuel cell stacks. The change in mass flow rate of the gas mixture inside the manifold can be represented as:

$$\begin{cases} \frac{dm_{H_2}}{dt} = \dot{m}_{ej,in,H_2} + \dot{m}_{bl,in,H_2} - \dot{m}_{out,H_2} \\ \frac{dm_{N_2}}{dt} = \dot{m}_{ej,in,N_2} + \dot{m}_{bl,in,N_2} - \dot{m}_{out,N_2} \end{cases} \tag{3}$$

In Equation (3), $\dot{m}_{ej,in,H_2}$, $\dot{m}_{bl,in,H_2}$, $\dot{m}_{ej,in,N_2}$, and $\dot{m}_{bl,in,N_2}$ are the mass flow rates of hydrogen and nitrogen entering the supply common rail from the ejector and recirculation blower, kg/s; $\dot{m}_{out,H_2}$ and $\dot{m}_{out,N_2}$ are the mass flow rates of hydrogen and nitrogen leaving the manifold and entering the fuel cell stacks, kg/s. The mass flow rates of the various gas components inside the exhaust common rail can be calculated similarly.

2.2.3. Proportional Valve Model

The flow characteristics of the proportional valve can be determined based on the Sanville flow-

pressure formula[10]. In terms of valve selection, it is necessary to meet the hydrogen injection flow rate required by the maximum current pulled by each fuel cell stack. The proportional valve diameters for the three fuel cell stacks are selected as 3 mm, 4 mm, and 5 mm.

2.2.4. Ejector Model

The ejector, as shown in Figure 2, accelerates and reduces the pressure of the primary flow, creating a pressure difference to allow the intake of the secondary flow. The primary flow and the secondary flow enter the mixer of the ejector and mix within it. The well-mixed gas then goes through the expansion section for deceleration and compression before flowing out.

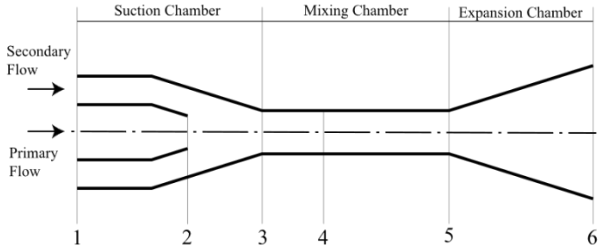

Figure 2: Schematic diagram of the ejector structure.[11]

To model the ejector, the following assumptions and simplifications[8, 11] are made:

(1) All gases are ideal gases.

(2) The radial velocity of primary flow is uniform at all locations in the primary flow.

(3) The pressure of the primary flow and the secondary flow is uniform radially at all locations.

(4) The primary flow and the secondary flow mix from node 3 to node 4, and the pressures of the primary flow and the secondary flow are equal at the mixing point.

(5) The inner wall of the ejector is adiabatic.

In the gas flow from node 1 to node 2 within the nozzle in Figure 2, the gas flow is generally in subsonic state. At this point, the gas mass flow rate and the Mach number at the nozzle can be calculated using Equations (4) and (5):

$$\dot{m}_p = P_p A_t \sqrt{\frac{2\psi_p k_{H_2}\left[\left(P_s/P_p\right)^{2/k_{H_2}} - \left(P_s/P_p\right)^{\left(k_{H_2}+1\right)/k_{H_2}}\right]}{\left(k_{H_2}-1\right)R_{H_2}T_p}} \tag{4}$$

$$Ma_t = \sqrt{\frac{2\left[1 - \left(P_s/P_p\right)^{\left(k_{H_2}-1\right)/k_{H_2}}\right]}{\left(k_{H_2}-1\right)}} \tag{5}$$

In Equations (4) and (5), $\dot{m}_p$ is the mass flow rate of the gas through the nozzle, kg/s, Ma_t is the Mach number at the nozzle; P_p is the pressure of the primary flow at the nozzle inlet, Pa; P_s is the pressure of the secondary flow at the nozzle outlet, Pa; ψ_p is the hydrogen specific heat ratio accounting for flow resistance inside the nozzle; k_{H_2} is the specific heat ratio of hydrogen; T_p is the gas temperature at the nozzle inlet, K.

Between node 2 and node 3 of Figure 2, based on the thermodynamic properties, Equations (6) to (8) can be used to calculate the gas pressure, temperature, velocity, and Mach number:

$$\frac{P_p}{P_{p,3}} = \left[1 + \frac{1}{2}\left(k_{H_2} - 1\right)Ma_{p,3}^2\right]^{k_p/(k_p-1)} \tag{6}$$

$$\frac{T_p}{T_{p,3}} = 1 + \frac{1}{2}\left(k_{H_2} - 1\right)Ma_{p,3}^2 \tag{7}$$

$$v_{p,3} = Ma_{p,3}\sqrt{k_{H_2}R_{H_2}T_{p,3}} \tag{8}$$

In Equations (6) to (8), $P_{p,3}$ is the pressure of the primary flow at node 3, Pa; $T_{p,3}$ is the temperature at node 3, K; $v_{p,3}$ is the gas velocity of the primary flow at node 3, m/s; $Ma_{p,3}$ is the Mach number of the primary flow at node 3.

The flow diameter of the primary flow at node 3 can be obtained from Equation (9):

$$\sqrt{\xi}\frac{D_{p,3}}{D_t} = \sqrt{\frac{Ma_t}{Ma_{p,3}}}\left[\frac{2 + \left(k_{H_2} - 1\right)Ma_{p,3}^2}{2 + \left(k_{H_2} + 1\right)Ma_t^2}\right]^{\left(k_{H_2}+1\right)/4\left(k_{H_2}-1\right)} \tag{9}$$

In Equation (9), $D_{p,3}$ is the flow diameter of the primary flow at node 3, m; D_t is the nozzle diameter, m; ξ is the friction loss coefficient between primary flow and secondary flow.

The velocity at node 3 is radially distributed according to a certain function. According to the reference [8], the mass flow rate of the secondary flow can be calculated as Equation (10):

$$\dot{m}_s = \frac{\pi\bar{\rho}_s v_{p,3}\left(D_m - D_{p,3}\right)\left[D_m + \left(n_v + 1\right)D_{p,3}\right]}{2\left(n_v + 1\right)\left(n_v + 2\right)} \tag{10}$$

In Equation (10), $\dot{m}_s$ is the mass flow rate of the secondary flow, kg/s; $\bar{\rho}_s$ is the average density of the secondary flow; D_m is the diameter of the mixer section of the ejector, m; n_v is a dimensionless coefficient that reflect the relationship between gas pressure and flow channel diameter..

After complete mixing, the gas maintains constant velocity, mass flow rate, temperature, and pressure from node 4 to 5. Besides, the pressure variation of the gas in the expansion section can also be obtained from thermodynamic formulas.

2.2.5. Hydrogen Recirculation Blower Model

The hydrogen recirculation blower's inlet is connected to the exhaust common rail, and its outlet is connected to the supply common rail.

According to reference [7], the correction method of blower speed is given by Equation (11):

$$\omega_{bl,c} = \frac{\omega_{bl}}{\sqrt{T_{rm}/T_{ref}}} \tag{11}$$

In Equation (11), ω_{bl} and $\omega_{bl,c}$ are the uncorrected and corrected recirculation blower speeds, rad/s; T_{rm} is the gas temperature in the exhaust pipe, K; T_{ref} is the reference temperature under standard conditions, taken as 288 K.

Hydrogen gas flow rate through the recirculation blower is shown in Equation (12):

$$\dot{m}_{bl,c} = \phi_{bl}\rho_{rm}\frac{1}{4}\pi d_{bl}^2 U_{bl} \tag{12}$$

In Equation (12), $\dot{m}_{bl,c}$ is the corrected gas mass flow rate through the recirculation blower, kg/s; ρ_{rm} is the gas density in the exhaust common rail; d_{bl} is the diameter of the recirculation blower, m; U_{bl} is the linear velocity at the tip of the rotor blades, m/s; ϕ_{bl} is a dimensionless parameter which can be obtained through fitting

The resistance torque experienced by the recirculation blower can be calculated as Equation (13).

$$M_{resistance} = \frac{c_{p,rm}T_{rm}\dot{m}_{bl}}{\omega_{bl}\eta_{bl}}\left[\left(\frac{P_{bl,out}}{P_{bl,in}}\right)^{(k_{rm}-1)/k_{rm}} - 1\right] \tag{13}$$

In Equation (13), $M_{resistance}$ is the resistance torque of the recirculation blower rotor, Nm; $\dot{m}_{bl}$ is the gas mass flow rate through the recirculation blower, kg/s; η_{bl} is the efficiency of the recirculation blower.

2.2.6. Gas-Water Separator Model

The gas-water separator can promptly collect liquid water and discharge it to prevent flooding in the fuel cell stack. Flow resistance can measure the pressure drop generated during the gas-water separation process. In this paper, a separation efficiency of 95% is assumed[12].

3. Hydrogen System Inlet Pressure Control and Controller Design

3.1. Control Problem Description

During the operation of a multi-stack fuel cell system, it is necessary to ensure that the hydrogen inlet pressure and cathode-side air inlet pressure maintain a certain pressure difference. Besides the pressure in supply common rail should be maintained. The main control objectives are as follows:

(1)Control the hydrogen flow rate in the supply common rail to maintain stable pressure.

(2)Control the hydrogen inlet pressure on the anode side of each stack to meet the pressure requirements, ensuring a certain pressure difference between the cathode and anode sides.

Model predictive control offers advantages such as robustness and fast dynamic response[13]. In this system, the proportional valves play a crucial role in supplying hydrogen to the common rail and anode flow channels of the fuel cell stack, making precise control of the inlet pressure essential.

3.1.1. Model Predictive Control and Prediction Model

The hydrogen system of a fuel cell is a typical nonlinear system. To predict its dynamic behavior effectively and reduce the difficulty of optimization problem-solving, this paper adopts the concept of local linearization. This paper uses system identification to establish local linearized models. System identification begins with defining the system's input signals and applying identification signals around the steady-state operating points to create a mathematical model of the system. Random signals are used as identification signals in this work.

In the hydrogen system of a fuel cell, four proportional valves, with opening degrees denoted as φ_1 to φ_4, are chosen as system inputs. The control variables are the supply common rail pressure and the inlet pressures of each fuel cell stack, denoted as $P_{commonal\,rail}$, P_{stack1}, P_{stack2} and P_{stack3}. Next, the

identification of the system's predictive model is carried out. Six steady-state points at 70 A, 110 A, 150 A, 180 A, 200 A, and 250 A are selected. As an example, the parameters for the actuator at 180 A are shown in Table 1.

Using the MATLAB Identification Toolbox, the system was identified based on the identification signal and system response. the system response under the identification signal at 180A is shown in Figure 3, and the identification fitting rates are shown in Table 2.

Table 1: Steady-State Parameters.

Parameters	steady-state value @180A	Min 160A	Max 200A
Proportional Valve 1 Opening	0.50	0.49	0.51
Proportional Valve 2 Opening	0.40	0.39	0.41
Proportional Valve 3 Opening	0.55	0.54	0.56
Proportional Valve 4 Opening	0.41	0.40	0.42

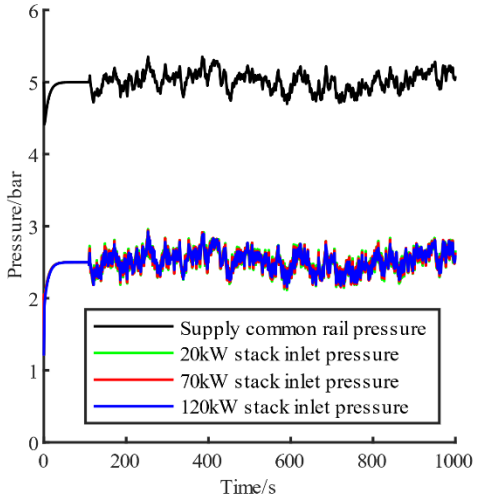

Figure 3: System Response under Identification Signal.

Table 2: Identification Results for the 180A Steady-State Point.

Parameters	Fitting Rate
Supply Common Rail Pressure	91.3%
20 kW Stack Inlet Pressure	78.6%
70 kW Stack Inlet Pressure	78.8%
120 kW Stack Inlet Pressure	79.4%

The fitting rates for the steady-state points are all above 75%. Therefore, it meets the requirements for controller design. The same process is applied to all the other steady-state points.

3.1.2. Controller Design

The four proportional valve opening signals are used as system inputs, the current of the three stacks as measurable disturbances, and the supply common rail pressure and the gas inlet pressure of the three stacks as system outputs. The sampling time, prediction horizon, and control horizon affect the performance of the model predictive controller. A sampling time of 0.1 s, a prediction horizon of 40, and a control horizon of 20 were selected.

Model predictive control requires trajectory planning for the reference trajectory. When the setpoint is set to a value , the expected value of the system can be expressed as Equation (14).

$$y_r(k) = y(k)$$
$$y_r(k+j) = \alpha y_r(k+j-1) + (1-\alpha)y_s \quad j = 1,2,\ldots,P \tag{14}$$

In Equation (14), y, y_r & y_s are the actual measured output, the reference trajectory & the setpoint; α is the smoothing factor, which takes values between 0 and 1; P is the prediction horizon.

Adjusting the smoothing factor α can change the shape of the reference trajectory. In this study, model predictive controllers were established for six steady-state points: 70A, 110A, 150A, 180A, 200A, and 250A with the range of 0-80A, 80-135A, 135-165A, 165-190A, 190-220A and 220-300A.

4. Results and Analysis

4.1. Effect and Comparison of Model Predictive Controller under Step Load Conditions

Under the model load conditions shown in Figure 4, the changes in common rail pressure and the pressure at the inlet of each fuel cell stack in the model can be observed.

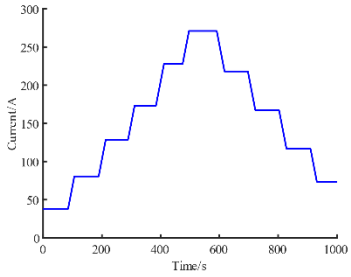

Figure 4: Load Current in Step-Like Condition.

The supply common rail pressure under PID and model predictive controllers is shown in Figure 5(a). From Figure 5(a), it can be observed that the model predictive controller exhibits better control performance, with smaller pressure fluctuations compared to the PID controller at the setpoint of 5 bar. Furthermore, as indicated in the zoomed-in graph, the opening and closing of the hydrogen exhaust valve can cause significant disturbances in the supply common rail pressure, resulting in pressure spikes. In such cases, the model predictive controller can still bring the supply common rail pressure back to the stable value in a shorter adjustment time, reflecting the good suitability for hydrogen pressure control in multi-stack fuel cell systems.

The changes in the inlet pressure of each fuel cell stack over time are shown in Figures 5(b) to (d). It can be observed that, when the load current changes, leading to fluctuations in the demand pressure, the model predictive controller results in smaller deviations between actual and desired pressures and shorter adjustment times. Taking the 70 kW fuel cell stack as an example, Figure 5(c) shows that the maximum deviation in actual inlet pressure under the PID controller is 0.008 bar, while under the model predictive controller, it is reduced to 0.0062 bar, a reduction of 22.5%. The adjustment time under the PID controller is 31 seconds, whereas it is shortened to 22 seconds under the model predictive controller. The result is more stable inlet pressure for the fuel cell stack with a shorter adjustment time, which can improve the efficiency and extend the lifespan of the fuel cell system.

Furthermore, as shown in Figure 7(d), because of larger fuel cell stacks, the disturbances caused by the exhaust valve have a slightly greater impact of larger pressure fluctuations. Figure 5(d) reveals that the pressure fluctuation caused by exhaust valve in the 120 kW fuel cell stack is slightly larger under the model predictive control than under the PID controller, the frequency is lower. Considering the model predictive controller's ability to bring the pressure back to the stable value in a shorter adjustment time, the model predictive controller still demonstrates superior performance.

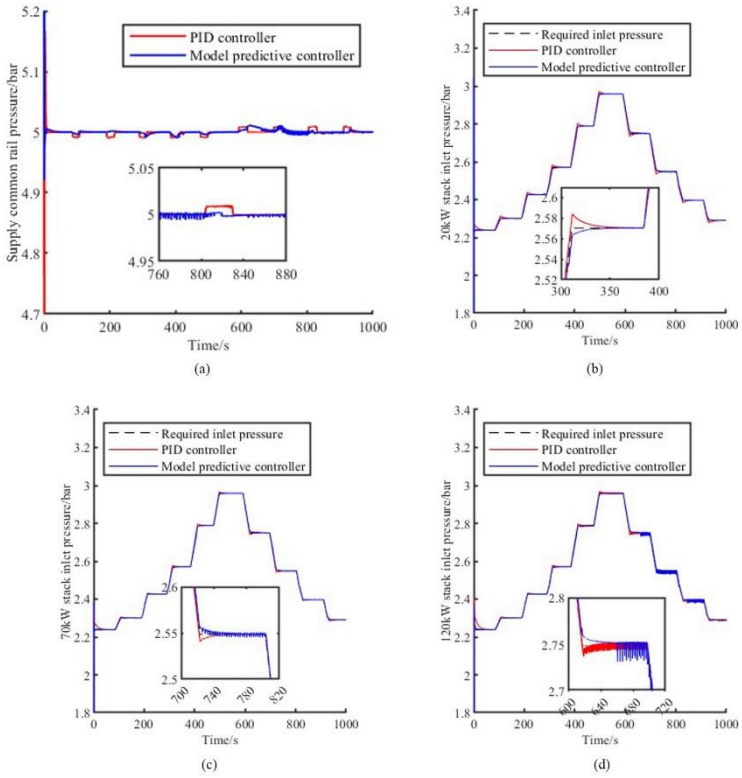

Figure 5. Hydrogen Pressure under PID and Model Predictive Controllers.

(a) Supply common rail Pressure.
(b) Inlet Hydrogen Pressure of the 20 kW Fuel Cell Stack.
(c) Inlet Hydrogen Pressure of the 70 kW Fuel Cell Stack.
(d) Inlet Hydrogen Pressure of the 120 kW Fuel Cell Stack.

4.2. Impact and Comparison of Model Predictive Controller on Hydrogen Recirculation Blower Operation under C-WTVC Condition

In this section, the current of the hydrogen system model under the C-WTVC (China World Transient Vehicle Cycle) condition will be observed to investigate the effect on the hydrogen recirculation blower's speed and power consumption.

The power consumption of the hydrogen recirculation blower under both controllers is presented in Table 3. After designing the model predictive controller, the power consumption of the recirculation blower decreases from 1715 kJ to 1481 kJ, a reduction of 13.6%. It is because the optimization of the inlet hydrogen pressure control has a particularly significant effect on reducing the blower's power consumption. As a result, the hydrogen recirculation blower's speed remains lower than that of the PID controller for most of the time. Thus, the model predictive controller results in lower parasitic power, contributing to an overall increase in system efficiency.

Table 3: Power Consumption of the Hydrogen Recirculation Blower.

	PID Controller	Model Predictive Controller
Power Consumption (kJ)	1 715	1 481

In conclusion, the model predictive controller outperforms the PID controller in terms of control effectiveness. It offers benefits such as reduced overshoot, robustness, and faster dynamic response. Additionally, it can lower parasitic power in the system, making it more suitable for the multi-stack fuel cell hydrogen system studied in this research.

5. Conclusion

This study focused on the issue of hydrogen inlet pressure control in multi-stack fuel cell systems, which has been less explored in existing research worldwide. Based on a multi-stack fuel cell hydrogen system with a supply and exhaust common rail structure, the system was modeled in Simulink. The model predictive controller was designed using a local linearization approach, where local linear models were established around different steady-state operating points, and the controller was switched accordingly. The simulation results led to the following conclusions:

(1) The model predictive controller exhibited smaller pressure fluctuations compared to the PID controller in supply common rail and pressure error was also smaller at step changes.

(2) The model predictive controller showed smaller deviations between actual and desired pressures compared to the traditional PID controller. For example, for the 70 kW stack, the maximum pressure deviation decreased by 22.5% and the adjustment time was reduced from 31 seconds to 22 seconds.

(3) Under the C-WTVC load condition, the model predictive controller led to lower power consumption of the recirculation blower, reducing it from 1715 kJ to 1481 kJ.

(4) The designed model predictive controller performed better than the traditional PID controller in hydrogen pressure control. This control method offers advantages such as smaller overshoot and robustness while also reducing parasitic power in the system, making it more suitable for the multi-stack fuel cell hydrogen system studied in this research, and it has practical applications.

References

[1] Qi Jing, Zhai Yunfeng, St-Pierre Jean. Effect of contaminant mixtures in air on proton exchange membrane fuel cell performance [J]. Journal of Power Sources, 2019, 413: 86-97.

[2] Zhou Su, Fan Lei, Zhang Gang, etc. A review on proton exchange membrane multi-stack fuel cell systems: architecture, performance, and power management [J], Applied Energy, 2022, 310: 118555.

[3] Yang Bo, Li Jiale, Li Yulin, etc. A critical survey of proton exchange membrane fuel cell system control: Summaries, advances, and perspectives [J]. International Journal of Hydrogen Energy, 2022, 47(17): 9986-10020.

[4] Nie Wei, Sun Zhen, Zhou Bingjie, etc. A study on hydrogen pressure control strategy of fuel cell power system [J]. Marine Electric & Electronic Engineering, 2021, 41(6): 6.

[5] Ding Tianwei, Huang Xing, Wang Yupeng, etc. Hydrogen control method for automotive fuel cell systems[C]//. Proceedings of China SAE congress (2), 2019: 366-371.

[6] Zhou Bingjie. Research of fuel cell power system cathode and anode pressure balance control strategy. University of Electronic Science and Technology of China, 2022. DOI: 10.27005/d.cnki.gdzku. 2022.001384.

[7] He Jinglin, Choe Song-Yul, Hong Chang-Oug. Analysis and control of a hybrid fuel delivery system for a polymer electrolyte membrane fuel cell [J]. Journal of Power Sources, 2008, 185(2):973-984.

[8] Zhang Jiaming, Ma Tiancai, Cong Ming, etc. Modeling and control of high-power fuel cell hydrogen systems [J]. Automobile Technology, 2021, 02: 23-27.

[9] J.T. Pukrushpan, A.G. Stefanopoulou, Huei Peng. Control of fuel cell breathing [J]. IEEE Control Systems, 2004, 24(2): 30-46.

[10] Edmond Richer, Yildirim Hurmuzlu. A high performance pneumatic force actuator system: Part I—Nonlinear mathematical model [J]. J. dyn. sys., meas., control, 2000, 122(3): 416-425.

[11] Mohsen Dadvar, Ebrahim Afshari. Analysis of design parameters in anodic recirculation system based on ejector technology for PEM fuel cells: A new approach in designing [J]. International Journal of Hydrogen Energy, 2014, 39: 12061-12073.

[12] Feng Jin, Ding Lingyun, Zhang Manlai, etc. Centrifugal gas-liquid separator main structural parameters analysis [J]. China Petroleum Machinery. 2007(02): 19-21+71.

[13] Chen Hong. Model predictive control [M]. Beijing: Science Press, 2013: 1-3.